Chaos, Solitons and Fractals 99 (2017) 256–262

Contents lists available at ScienceDirect

Chaos, Solitons and Fractals

Nonlinear Science, and Nonequilibrium and Complex Phenomena

journal homepage: www.elsevier.com/locate/chaos

Application of rotational spectrum for correlation dimension estimation

Martin Dlask*, Jaromir Kukal

Czech Technical University, Faculty of Nuclear Sciences and Physical Engineering, Department of Software Engineering, Trojanova 12, Prague, Czech Republic

ARTICLE INFO

Article history:
Received 22 May 2016
Revised 15 January 2017
Accepted 12 April 2017
Available online 17 April 2017

MSC:
28A80
65P20

Keywords:
Point set
Correlation dimension
Power spectrum
Rotation
Monte Carlo

ABSTRACT

Correlation dimension is one of the many types of fractal dimension. It is usually estimated from a finite number of points from a fractal set using correlation sum and regression in a log-log plot. However, this traditional approach requires a large amount of data and often leads to a biased estimate. The novel approach proposed here can be used for the estimation of the correlation dimension in a frequency domain using the power spectrum of the investigated fractal set. This work presents a new spectral characteristic called "rotational spectrum" and shows its properties in relation to the correlation dimension. The theoretical results can be directly applied to uniformly distributed samples from a given point set. The efficiency of the proposed method was tested on sets with a known correlation dimension using Monte Carlo simulation. The simulation results showed that this method can provide an unbiased estimation for many types of fractal sets.

© 2017 Elsevier Ltd. All rights reserved.

1. Introduction

Correlation dimension D_2 is a popular tool for fractal dimension estimation and belongs to a family of entropy-based fractal dimensions such as capacity dimension D_0, information dimension D_1 and their generalisation, Renyi dimension D_α, for $\alpha \geq 0$. The properties of the different dimension types are summarised in [1] and [2]. The main idea of using correlation dimension is the distance between its points in space. In the original concept, only the number of points that are not farther apart as a fixed value can carry the information about the density of points contained in the investigated set. The geometrical meaning of correlation dimension is explained well in [3].

This traditional approach of correlation dimension estimation is based on Grassberger and Procaccia's algorithm [4,5] and is widely used in biomedicine for electroencephalography signal analysis [6,7] or in cardiology [8]. Recently, new approaches of correlation dimension estimation were presented using a weighting function [9] or methods suitable for high-dimensional signals [10]. The linear regression model, on which the majority of methods are based, provides an often biased estimate of fractal dimension; for this reason, Hongying and Duanfeng [11] made some efforts to improve this procedure.

In this work, we present a novel approach of correlation dimension estimation that is based on the rotation of the power spectrum of a point set. The proposed method is stable even for a small number of points, and the resulting characteristic has a smooth development.

2. Correlation dimension

Correlation dimension, introduced by Grassberger and Procaccia, involves measuring the distance between all pairs of points in the investigated set. For the Lebesgue measurable set $\mathcal{F} \subset \mathbb{R}^n$, the *correlation sum* [4] is defined for $r > 0$ as the limit case

$$C(r) = \lim_{N\to\infty} \frac{2}{N(N-1)} \sum_{i=1}^{N-1} \sum_{j=i+1}^{N} I(\|\boldsymbol{x_i} - \boldsymbol{x_j}\| \leq r), \tag{1}$$

where $\|\cdot\|$ denotes a Euclidean norm that is rotation invariant, I is the indicator function and $\boldsymbol{x}_1, \ldots, \boldsymbol{x}_N$ are vectors from $\mathcal{F}$. Because the correlation dimension expresses the relative amount of points whose distance is less than r, the correlation sum can be rewritten as

$$C(r) = \mathop{E}_{\boldsymbol{x},\boldsymbol{y}\sim U(\mathcal{F})} I(\|\mathbf{x} - \mathbf{y}\| \leq r) = \mathop{\text{prob}}_{\boldsymbol{x},\boldsymbol{y}\sim U(\mathcal{F})} (\|\boldsymbol{x} - \boldsymbol{y}\| \leq r), \tag{2}$$

for $\boldsymbol{x}, \boldsymbol{y}$ that are uniformly distributed on $\mathcal{F}$. Therefore, $C(r)$ is a cumulative distribution function of random variable $r = \|\boldsymbol{x} - \boldsymbol{y}\|$. The

* Corresponding author.
E-mail address: martindlask@centrum.cz (M. Dlask).

http://dx.doi.org/10.1016/j.chaos.2017.04.026
0960-0779/© 2017 Elsevier Ltd. All rights reserved.

correlation dimension D_2 of set $\mathcal{F}$ is based on the correlation sum and is defined as

$$D_2 = \lim_{r\to 0^+} \frac{\ln \mathrm{C}(r)}{\ln r}, \tag{3}$$

if the limit exists.

3. Continuous spectrum of a point set

The Fourier transform of an n-dimensional set $\mathcal{F} \subset \mathbb{R}^n$ is defined using the operator of the expected value [12] as

$$\mathrm{F}(\boldsymbol{\omega}) = \mathop{\mathrm{E}}_{\boldsymbol{x}\sim \mathrm{U}(\mathcal{F})} \exp(-\mathrm{i}\boldsymbol{\omega}\cdot\boldsymbol{x}) \tag{4}$$

for angular frequency $\boldsymbol{\omega} \in \mathbb{R}^n$ and for $\boldsymbol{x}$ uniformly distributed on $\mathcal{F}$. The *power spectrum* of set $\mathcal{F}$ equals $\mathrm{P}(\boldsymbol{\omega}) = |\mathrm{F}(\boldsymbol{\omega})|^2 = \mathrm{F}(\boldsymbol{\omega})\cdot \mathrm{F}^*(\boldsymbol{\omega})$, where F^* is a complex conjugate of F. Moreover, it can be expressed as

$$\begin{aligned}\mathrm{P}(\boldsymbol{\omega}) &= \mathop{\mathrm{E}}_{\boldsymbol{x}\sim \mathrm{U}(\mathcal{F})} \mathop{\mathrm{E}}_{\boldsymbol{y}\sim \mathrm{U}(\mathcal{F})} \exp(-\mathrm{i}\boldsymbol{\omega}\cdot\boldsymbol{x}) \exp(\mathrm{i}\boldsymbol{\omega}\cdot\boldsymbol{y}) \\ &= \mathop{\mathrm{E}}_{\boldsymbol{x},\boldsymbol{y}\sim \mathrm{U}(\mathcal{F})} \exp(-\mathrm{i}\boldsymbol{\omega}\cdot(\boldsymbol{x}-\boldsymbol{y})),\end{aligned} \tag{5}$$

where $\boldsymbol{x}$ and $\boldsymbol{y}$ are independent and identically distributed from $\mathcal{F}$. The power spectrum is frequently used for fractal set investigation [13–15]. When the research is physically motivated, it is usual to denote the angular frequency as $\omega = 2\pi/\lambda$ for wavelength λ of an X-ray or light beam.

4. Rotational spectrum

The goal of the novel method is to obtain a one-dimensional function as a derivative of the power spectrum, which is useful in fractal analysis. The procedure was inspired by Debye [16] and by his X-ray diffraction method, which is often referred to as the Debye-Scherrer method. We denote $\mathrm{SO}(n)$ as the group of all rotations in $\mathbb{R}^n$ around the origin. Because any rotation $\mathrm{R} \in \mathrm{SO}(n)$ is a linear transform, the following equation holds

$$\mathrm{R}(\boldsymbol{x}) - \mathrm{R}(\boldsymbol{y}) = \mathrm{R}(\boldsymbol{x}-\boldsymbol{y}) = \|\boldsymbol{x}-\boldsymbol{y}\|\cdot\boldsymbol{\xi}, \tag{6}$$

where $\boldsymbol{\xi}$ is a direction vector satisfying $\|\boldsymbol{\xi}\| = 1$ and $\boldsymbol{\xi} \in \mathcal{S}_{n-1}$ for an n-dimensional sphere $\mathcal{S}_{n-1} = \{\boldsymbol{x} \in \mathbb{R}^n : \|\boldsymbol{x}\| = 1\}$. Using the factorisation of angular frequency $\boldsymbol{\omega} = \Omega\cdot\boldsymbol{\psi}$ for $\Omega \in \mathbb{R}_0^+$ and normalisation vector $\boldsymbol{\psi} \in \mathcal{S}_{n-1}$, we can define *rotational spectrum* as

$$\mathrm{S}(\Omega) = \mathop{\mathrm{E}}_{\mathrm{R}\in \mathrm{SO}(n)} \mathop{\mathrm{E}}_{\boldsymbol{\psi}\in\mathcal{S}_{n-1}} \mathop{\mathrm{E}}_{\boldsymbol{x},\boldsymbol{y}\sim \mathrm{U}(\mathcal{F})} \exp(-\mathrm{i}\Omega\boldsymbol{\psi}\mathrm{R}(\boldsymbol{x}-\boldsymbol{y})), \tag{7}$$

which can be expressed explicitly in the following theorem.

Theorem 1. *Rotational spectrum can be expressed as*

$$\mathrm{S}(\Omega) = \mathop{\mathrm{E}}_{\boldsymbol{x},\boldsymbol{y}\sim \mathrm{U}(\mathcal{F})} \mathrm{H}_n(\Omega\|\boldsymbol{x}-\boldsymbol{y}\|), \tag{8}$$

where

$$\mathrm{H}_n(q) = \frac{2^{\frac{n-2}{2}}\cdot\Gamma\left(\frac{n}{2}\right)}{q^{\frac{n-2}{2}}} \mathrm{J}_{\frac{n-2}{2}}(q). \tag{9}$$

Proof. Because every rotation is a linear transform, we can rewrite the rotational spectrum as

$$\mathrm{S}(\Omega) = \mathop{\mathrm{E}}_{\boldsymbol{x},\boldsymbol{y}\sim \mathrm{U}(\mathcal{F})} \mathop{\mathrm{E}}_{\boldsymbol{\psi},\boldsymbol{\xi}\in\mathcal{S}_{n-1}} \exp(-\mathrm{i}\Omega\|\boldsymbol{x}-\boldsymbol{y}\|\boldsymbol{\psi}\cdot\boldsymbol{\xi}). \tag{10}$$

The angle ν between vectors $\boldsymbol{\psi}$ and $\boldsymbol{\xi}$ satisfies $\cos\nu = \boldsymbol{\psi}\cdot\boldsymbol{\xi}$. Without loss of generality, we can set $\boldsymbol{\xi} = (1, 0, 0, \ldots, 0)$ and rewrite the rotational spectrum as

$$S(\Omega) = \mathop{\mathrm{E}}_{\boldsymbol{x},\boldsymbol{y}\in\mathcal{F}} H_n(\Omega\|\boldsymbol{x}-\boldsymbol{y}\|), \tag{11}$$

where the function $\mathrm{H}_n : \mathbb{R} \mapsto \mathbb{C}$ is defined as

$$\mathrm{H}_n(q) = \mathop{\mathrm{E}}_{\substack{\boldsymbol{\psi}\in\mathcal{S}_{n-1}\\ \psi_1=\cos\nu}} \exp(-\mathrm{i}q\cos\nu). \tag{12}$$

For $n = 1$, we obtain a degenerated rotation together with $\nu \in \{0, \pi\}$; therefore, the kernel function H_1 equals

$$\mathrm{H}_1(q) = \frac{\exp(-\mathrm{i}q) + \exp(\mathrm{i}q)}{2} = \cos q. \tag{13}$$

In case $n \geq 2$, we can express the kernel function using an integral formula:

$$\mathrm{H}_n(q) = \frac{\mathrm{I}_1(q)}{\mathrm{I}_2(q)} = \frac{\int_0^\pi \exp(-\mathrm{i}q\cos\nu)\sin^{n-2}\nu\,\mathrm{d}\nu}{\int_0^\pi \sin^{n-2}\nu\,\mathrm{d}\nu}. \tag{14}$$

The Poisson integral [17] formula for the Bessel function $\mathrm{J}_p(q)$ of the first kind in the form

$$\mathrm{J}_p(q) = \frac{\left(\frac{q}{2}\right)^p}{\Gamma\left(p+\frac{1}{2}\right)\sqrt{\pi}} \int_0^\pi \exp(-\mathrm{i}q\cos\nu)\sin^{2p}\nu\,\mathrm{d}\nu \tag{15}$$

allows the integral in the nominator to be rewritten as

$$\mathrm{I}_1(q) = \frac{\mathrm{J}_p(q)\Gamma\left(p+\frac{1}{2}\right)\sqrt{\pi}}{\left(\frac{q}{2}\right)^p}, \tag{16}$$

whereas the integral in the denominator is a limit case of the Poisson formula

$$\mathrm{I}_2(q) = \lim_{q\to 0} \frac{\mathrm{J}_p(q)\Gamma\left(p+\frac{1}{2}\right)\sqrt{\pi}}{\left(\frac{q}{2}\right)^p} = \frac{\Gamma\left(p+\frac{1}{2}\right)\sqrt{\pi}}{\Gamma(p+1)}. \tag{17}$$

For $p = \frac{n-2}{2}$, we obtain the final form of the kernel function expressed by the Bessel function $\mathrm{J}_p(q)$ as

$$\mathrm{H}_n(q) = \frac{2^{\frac{n-2}{2}}\cdot\Gamma\left(\frac{n}{2}\right)}{q^{\frac{n-2}{2}}} \mathrm{J}_{\frac{n-2}{2}}(q). \tag{18}$$

Applying $\mathrm{H}_n(q)$ for $n = 1$, we obtain $\mathrm{H}_1(q) = \cos q$ as a particular case, which extends the range of formula (18) to $n \in \mathbb{R}$. □

The rotation can be performed in any space whose dimension n is not less than the dimension m of the original space of $\mathcal{F}$. When the dimension of the rotation is greater than m, any vector $\boldsymbol{x} \in \mathcal{F}$ is completed, with the zeros for the remaining $n-m$ coordinates having a sufficient length. The most valuable result can be obtained in the case of rotation in an infinite-dimensional space.

Theorem 2. *The scaled limit case of the kernel function* H_n *is the Gaussian function, i.e.,*

$$\lim_{n\to\infty} \mathrm{H}_n(t\sqrt{n}) = \exp\left(-\frac{t^2}{2}\right). \tag{19}$$

Proof. For the investigation of the behaviour of the kernel function when $n \to \infty$, we use the Taylor expansion of $H_n(q)$ centred at $q_0 = 0$

$$\mathrm{H}_n(q) = \sum_{k=0}^{\infty} \frac{\Gamma(\frac{n}{2})}{\Gamma(\frac{n}{2}+k)k!}\left(-\frac{q^2}{4}\right)^k, \tag{20}$$

and by using the substitution $q = t\sqrt{n}$, we can transform it into

$$\mathrm{H}_n(t\sqrt{n}) = \sum_{k=0}^{\infty} \frac{1}{k!}\left(-\frac{t^2}{2}\right)^k \frac{\Gamma(\frac{n}{2})n^k}{\Gamma(\frac{n}{2}+k)2^k}. \tag{21}$$

For every $k \in \mathbf{N}$, it holds that

$$\lim_{n\to\infty} \frac{\Gamma(\frac{n}{2})n^k}{\Gamma(\frac{n}{2}+k)2^k} = 1, \tag{22}$$

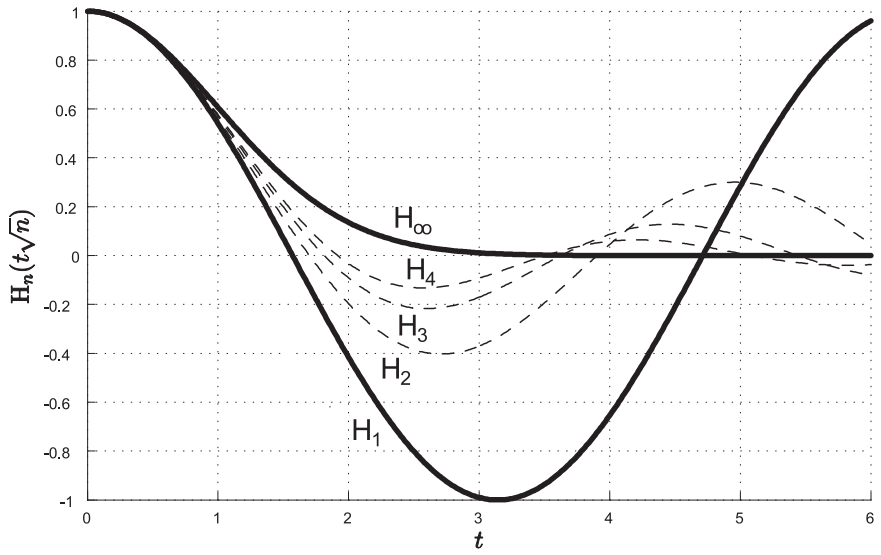

Fig. 1. Kernel functions of a rotational spectrum.

and, therefore, the limit case of the kernel function equals

$$\lim_{n\to\infty} \mathrm{H}_n(t\sqrt{n}) = \exp\left(-\frac{t^2}{2}\right). \tag{23}$$

□

For simplicity, we will use the following notation in the subsequent sections:

$$\mathrm{H}_\infty(q) = \exp\left(-\frac{q^2}{2}\right). \tag{24}$$

This type of Gaussian kernel has been widely applied in the Parzen density estimates [18–20] of a probability density function and its properties, but with another meaning and motivation. The behaviour of the $\mathrm{H}_n(q)$ kernels is visualised in Fig. 1 for various dimensions.

5. Relationship to correlation dimension

In this section, we discuss the relationship between the rotational spectrum for the limit kernel H_∞ and the correlation dimension. The correlation sum is a cumulative distribution function of the distances between the points in a fractal set; therefore, the rotational spectrum can be written as a Stieltjes integral:

$$\mathrm{S}(\Omega) = \int_0^\infty \mathrm{H}_\infty(\Omega r)\mathrm{dC}(r) = \int_0^\infty \exp\left(-\frac{\Omega^2 r^2}{2}\right)\mathrm{dC}(r). \tag{25}$$

After the application of the integration by parts, we can obtain

$$\mathrm{S}(\Omega) = \int_0^\infty \Omega^2 r \exp\left(-\frac{\Omega^2 r^2}{2}\right)\mathrm{C}(r)\Omega \mathrm{d}r, \tag{26}$$

and by substituting $\xi = \Omega r$, we get the integral formula for the rotational spectrum:

$$\mathrm{S}(\Omega) = \int_0^\infty \xi \cdot \mathrm{C}\left(\frac{\xi}{\Omega}\right)\exp\left(-\frac{\xi^2}{2}\right)\mathrm{d}\xi. \tag{27}$$

Theorem 3. *Let $\mathcal{F} \subset \mathbb{R}^n$ be a Lebesgue measurable set with the rotational spectrum*

$$\mathrm{S}(\Omega) = \underset{\boldsymbol{x},\boldsymbol{y}\sim\mathrm{U}(\mathcal{F})}{E} \mathrm{H}_\infty(\Omega\|\boldsymbol{x}-\boldsymbol{y}\|), \tag{28}$$

and let us assume that correlation dimension D_2 (3) exists. Then, it holds that

$$\lim_{\Omega\to\infty} \frac{\ln \mathrm{S}(\Omega)}{\ln \Omega} = -D_2. \tag{29}$$

Proof. To prove this, let us suppose that $\delta < 1$ and that, at first, $r < \delta$. Owing to the existence of correlation dimension, we have $\forall\epsilon > 0\, \exists\delta > 0$

$$0 < r < \delta \Rightarrow \left|\frac{\ln \mathrm{C}(r)}{\ln r} - D_2\right| < \epsilon,$$

and, therefore,

$$r^{D_2+\epsilon} < \mathrm{C}(r) < r^{D_2-\epsilon}. \tag{30}$$

However, for $r \geq \delta$, we have

$$\delta^{D_2+\epsilon} < C(r) \leq 1. \tag{31}$$

Now, we can estimate the lower and the upper boundary for the spectrum

$$\begin{aligned} S(\Omega) &= \underset{\boldsymbol{x},\boldsymbol{y}\sim\mathrm{U}(\mathcal{F})}{E} \exp\left(-\Omega^2\frac{\|\boldsymbol{x}-\boldsymbol{y}\|^2}{2}\right) \\ &= \int_0^\infty C(r)\Omega^2 r \exp\left(-\Omega^2\frac{r^2}{2}\right)\mathrm{d}r \end{aligned} \tag{32}$$

as

$$\mathrm{I_L}(\Omega) < \mathrm{S}(\Omega) < \mathrm{I_U}(\Omega). \tag{33}$$

We can rewrite $\mathrm{I_U}$ as

$$\begin{aligned} \mathrm{I_U}(\Omega) = &\int_0^\delta r^{D_2-\epsilon}\Omega^2 r \exp\left(-\frac{\Omega^2 r^2}{2}\right)\mathrm{d}r \\ &+ \int_\delta^\infty \Omega^2 r \exp\left(-\frac{\Omega^2 r^2}{2}\right)\mathrm{d}r, \end{aligned} \tag{34}$$

and after the substitution $t = \Omega^2 r^2/2$, we get

$$\mathrm{I_U}(\Omega) = \Omega^{\epsilon-D_2}\cdot 2^{\frac{D_2-\epsilon}{2}}\cdot\int_0^{\Omega^2\delta^2/2} t^{\frac{D_2-\epsilon}{2}}\exp(-t)\mathrm{d}t + \exp\left(\frac{-\Omega^2\delta^2}{2}\right). \tag{35}$$

Therefore, the upper bound $\mathrm{I_U}$ can be expressed as

$$\mathrm{I_U}(\Omega) = \left(\frac{\sqrt{2}}{\Omega}\right)^{D_2-\epsilon}\cdot\frac{D_2-\epsilon}{2}\cdot\Gamma_{\mathrm{inc}}\left(\frac{\Omega^2\delta^2}{2}, \frac{D_2-\epsilon}{2}\right), \tag{36}$$

where Γ_{inc} is an incomplete Gamma function. It is possible to do an estimation from above as

$$\mathrm{I_U} < \left(\frac{\sqrt{2}}{\Omega}\right)^{D_2-\epsilon}\cdot\frac{D_2-\epsilon}{2}\cdot\Gamma\left(\frac{D_2-\epsilon}{2}\right). \tag{37}$$

The lower bound I_L is rewritten as

$$I_L(\Omega) = \int_0^{\delta} r^{D_2+\epsilon}\Omega^2 r \exp\left(-\frac{\Omega^2 r^2}{2}\right)\mathrm{d}r + \int_{\delta}^{\infty} r^{D_2-\epsilon}\Omega^2 r \exp\left(-\frac{\Omega^2 r^2}{2}\right)\mathrm{d}r \tag{38}$$

and can be estimated as

$$I_L(\Omega) > \left(\frac{\sqrt{2}}{\Omega}\right)^{D_2+\epsilon} \cdot \Gamma_{\mathrm{inc}}\left(\frac{\Omega^2\delta^2}{2}, \frac{D_2+\epsilon}{2}+1\right). \tag{39}$$

Altogether, we receive the upper and the lower boundary for the logarithm of the rotational spectrum

$$(D_2-\epsilon)\left(\frac{1}{2}\ln 2 - \ln\Omega\right) + L_1(\Omega) > \ln S(\Omega) > (D_2+\epsilon)\left(\frac{1}{2}\ln 2 - \ln\Omega\right) + L_2(\Omega) \tag{40}$$

and after the rearrangement

$$-\epsilon + \frac{L_2(\Omega) + \frac{D_2+\epsilon}{2}\ln 2}{\ln\Omega} < \frac{S(\Omega)}{\ln\Omega} + D_2 < \epsilon + \frac{L_1(\Omega) + \frac{D_2-\epsilon}{2}\ln 2}{\ln\Omega} \tag{41}$$

for the functions

$$L_1(\Omega) = \ln\Gamma\left(\frac{D_2-\epsilon}{2}\right) + \ln\frac{D_2-\epsilon}{2} \tag{42}$$

and

$$L_2(\Omega) = \ln\Gamma_{\mathrm{inc}}\left(\frac{\Omega^2\delta^2}{2}, \frac{D_2+\epsilon}{2}+1\right). \tag{43}$$

It holds that both L_1 and L_2 are constrained functions of Ω. Therefore, Ω_0 exists, which guarantees that, for any $\Omega > \Omega_0 > 1$, it is valid that

$$\left|\frac{\ln S(\Omega)}{\ln\Omega} + D_2\right| < 2\epsilon = \epsilon^*, \tag{44}$$

which completes the proof. □

The Lebesgue measurability of the investigated set is an important prerequisite because it ensures the capability to perform a uniform sampling. As a general remark, we could consider another kernel function instead of H_∞. For any non-increasing function $\Phi : \mathbb{R}_0^+ \mapsto [0;1]$ satisfying $\Phi(0)=1$ and $\Phi(\infty)=0$, and whose first derivative $\Phi'(\xi)$ exists for any $\xi > 0$, we consider the rotational spectrum in a more general form as

$$S(\Omega) = \mathop{\mathrm{E}}_{\boldsymbol{x},\boldsymbol{y}\sim \mathrm{U}(\mathcal{F})} \Phi(\Omega\|\boldsymbol{x}-\boldsymbol{y}\|). \tag{45}$$

The Ψ function is defined as

$$\Psi(\alpha) = -\int_0^{\infty} \xi^{\alpha}\Phi'(\xi))\mathrm{d}\xi, \tag{46}$$

and the existence of limit (29) is guaranteed only if both $\Psi(D_2+\epsilon)$ and $\Psi(D_2-\epsilon)$ are finite for arbitrary $\epsilon \in (0;\epsilon_0)$s. Another example of a kernel function could be the generalised exponential kernel

$$\Phi_1(\xi) = \exp\left(-\frac{\xi^{\beta}}{\beta}\right) \tag{47}$$

for $\beta > 0$ or the inverse polynomial kernel

$$\Phi_2(\xi) = \frac{1}{P(\xi)}, \tag{48}$$

where $P(\xi)$ represents a polynomial of order $M > D_2 + 1$.

6. Method of estimation

The simulation of the rotational spectrum is based on generating point pairs using a Monte Carlo approach. The points are independently and uniformly sampled from the analysed set $\mathcal{F}$. With $M \in \mathbb{N}$ fixed and $\boldsymbol{x}_i, \boldsymbol{y}_i \sim \mathrm{U}(\mathcal{F})$, the rotational spectrum is estimated as

$$\widehat{S}(\Omega) = \frac{1}{M}\sum_{j=1}^{M} H_\infty(\Omega\|\boldsymbol{x}_j - \boldsymbol{y}_j\|) \tag{49}$$

including the variance estimate

$$\widehat{\mathrm{var}\,S}(\Omega) = \frac{1}{M-1}\sum_{j=1}^{M}(H_\infty\left(\Omega\|\boldsymbol{x}_j-\boldsymbol{y}_j\|\right) - \widehat{S}(\Omega))^2 \tag{50}$$

To take advantage of the linear dependence between the logarithm of the rotational spectrum and the logarithm of the distance, we can reasonably consider the model

$$\ln S(\Omega) = A - D_2 \cdot \ln\,\Omega + \epsilon. \tag{51}$$

The estimation of parameter D_2 is based on the maximum likelihood method using L_p regression with a minimisation criterion

$$CRIT = \sum_{k=1}^{N} |y_k - f(x_k, \boldsymbol{a})|^p \tag{52}$$

for $p > 1$ and a general model formulated as $y = f(x_k, \boldsymbol{a})$. In our case, the minimisation criterion satisfies

$$CRIT^* = \sum_{k=1}^{N} \left|\ln\,\widehat{S}(\Omega_k) - A + D_2 \ln\,\Omega_k\right|^p. \tag{53}$$

The algorithm is based on the capability to generate point pairs uniformly from a fractal set and can be formulated as follows:

- The parameter M is chosen arbitrarily, but is large enough (e.g., $M = 10^5$). This parameter represents the number of Monte Carlo simulations, which is equal to the number of point pairs from the fractal set used for the estimation.
- The values of Ω, in which the calculation is performed, are determined. For the simulation, it is recommended to choose regular sampling from the interval, where the rotational spectrum is expected to have a linear characteristic.
- The calculation of the rotational spectrum is performed at points $\Omega_1, \Omega_2 \ldots, \Omega_N$, according to Eq. (49).
- With the values of Ω_i and the respective $\widehat{S}(\Omega_i)$ estimates, it is possible to perform minimisation using Eq. (53) with a maximum likelihood method.
- The resulting parameter D_2 represents the estimate of the correlation dimension.

7. Application to simulated data

The main feature of the proposed methodology is its smoother dependence of the spectrum on Ω. We tested this property on point sets with well-known Hausdorff dimension, which are summarised in Table 1. On the left side of Fig. 2, there is a traditional log-log plot, where the logarithm of the correlation sum is plotted against the logarithm of the distances. The lines represent the upper and the lower theoretical bounds for $C(r)$. The right side of the figure shows the dependence of the logarithm of the infinite-dimensional rotational spectrum on the logarithm of the frequency (Ω). The experiment was performed on a two-dimensional Cantor dust with the contraction coefficient $a = 1/3$ and $M = 10^5$ pairs of points.

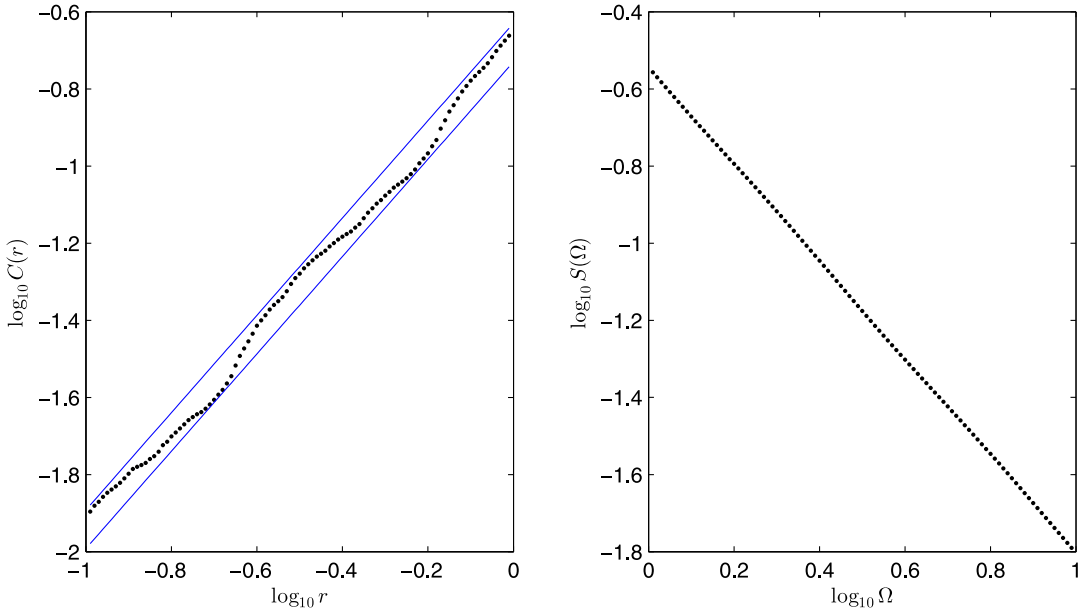

Fig. 2. Sample from the two-dimensional Cantor dust: correlation sum (left), rotational spectrum (right).

Table 1
List of point sets.

Structure	n	Parameter	Value	D_2
Cantor dust [21]	1–3	a	1/20–1/2	$-n \ln 2 / \ln a$
Levy flight trajectory [22]	2–4	α	0.2–1.0	$\min(\alpha, n)$
fBm trajectory [22]	3–4	H	0.25–0.75	$\min\left(\frac{1}{H}, n\right)$
fBm graph [23]	1	H	0.1–0.9	$2 - H$
Takagi function graph [24]	1	a	0.55–0.95	$2 + \log_2 a$

Table 2
Cantor dust analysis using linear least squares fitting.

M	Correlation sum			Rotational spectrum		
	$\widehat{D_2}$	sd	p-value	$\widehat{D_2}$	sd	p-value
10^3	1.2254	0.0648	0.2868	1.2501	0.0323	0.3579
10^4	1.2392	0.0202	0.1310	1.2689	0.0183	0.3502
10^5	1.2513	0.0039	0.0034	1.2592	0.0030	0.1915
10^6	1.2599	0.0005	$4.44 \cdot 10^{-5}$	1.2601	0.0003	$1.54 \cdot 10^{-7}$

Table 3
Cantor dust analysis using L_4.

M	Correlation sum			Rotational spectrum		
	$\widehat{D_2}$	sd	p-value	$\widehat{D_2}$	sd	p-value
10^3	1.2941	0.1178	0.3922	1.2378	0.1010	0.4059
10^4	1.2937	0.0803	0.3459	1.3019	0.0470	0.1971
10^5	1.2341	0.0574	0.3143	1.2618	0.0100	0.4976
10^6	1.2654	0.0474	0.4702	1.2609	0.0076	0.4498

The reason for the smooth development of the rotational spectrum characteristic is the infinite-dimensional rotation. It is possible to compare the correlation dimension estimate from the rotational spectrum approach and the traditional correlation sum. At first, the linear regression with least squares minimisation criterion was used to fit the model. However, the results were biased for a larger number of data points, as can be seen from Table 2. To avoid the bias, we decided to use L_p regression for the rotational spectrum fitting using a maximum likelihood method. The numerical experiments proved that any order $p \geq 4$ is appropriate to fit the model. Therefore, we considered L_4 regression for the estimation of the correlation dimension. Table 3 shows the results for different numbers of point pairs M. The estimates of $\widehat{D_2}$ based on L_4 regression were unbiased for both the correlation sum and the rotational spectrum. However, the variance of spectrum-based estimates rapidly decreased with M.

Table 4
Sierpinski carpet analysis for the different kernel functions.

Kernel function	D_2	$\widehat{D_2}$	sd	p-value	$f_{\min}$	$f_{\max}$
H_2	1.8928	1.9851	0.2625	0.4106	1.0	3.0
H_4	1.8928	1.8673	0.1128	0.3624	1.0	3.0
H_7	1.8928	1.9148	0.0863	0.3993	1.0	3.0
H_{10}	1.8928	1.9019	0.0636	0.4431	1.0	3.0
H_∞	1.8928	1.8958	0.0559	0.4784	1.0	3.0

It is also possible to estimate the rotational spectrum for finite rotation using the kernel functions H_n for $n \in \mathbb{N}$. The comparison of the kernel functions that can be used for the rotation of the power spectrum is shown in Fig. 3 for H_2, H_3, H_4 and H_∞. The traditional Sierpinski carpet was used for this simulation.

The estimation of the correlation dimension using different kernel functions can vary. The estimation of the dimension for the Sierpinski carpet for different kernel functions is presented in Table 4. The table shows the theoretical dimension D_2 based on the parameters and its estimate $\widehat{D_2}$ together with the standard deviation sd. The recommended Ω range for L_4 regression is also included, where $f_{\min} = \log_{10} \Omega_{\min}$ and $f_{\max} = \log_{10} \Omega_{\max}$.

With the increasing dimension of the kernel function H_n, the standard deviation decreased. The estimates were unbiased in all cases; however, the most accurate estimation occurred for H_∞. The recommended intervals for the regression were the same in all cases, which means that they were independent of the kernel function; nevertheless, as will be seen later, they will be dependent on the theoretical dimension of the fractal structure.

All of the subsequent numerical experiments were performed in MATLAB by means of Monte Carlo simulation for $M = 10^5$ point pairs. At first, we tested the methodology for correlation dimension estimation for an n-dimensional Cantor dust with contraction coefficient a. This methodology provided an unbiased estimation of the correlation dimension in the whole range of possible theoretical dimensions for different contraction coefficients a. Almost the same behaviour was exhibited in the estimation of the corre-

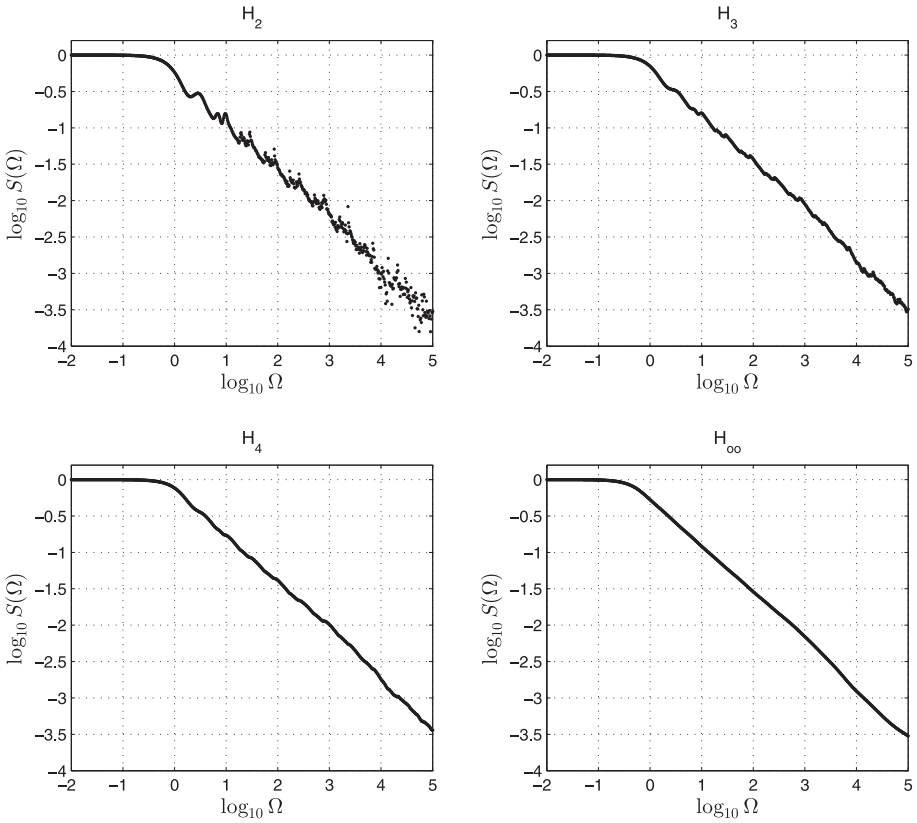

Fig. 3. Rotational spectra of the Sierpinski carpet.

Table 5
Analysis of the fractal sets with known dimension.

System	Parameters	D_2	$\widehat{D_2}$	*sd*	$f_{\min}$	$f_{\max}$
Cantor set	$a = 1/5,\ n = 1$	0.4307	0.4298	0.0396	0.0	2.0
Cantor set	$a = 1/3,\ n = 3$	1.8929	1.9065	0.0148	0.0	2.0
Levy flight	$\alpha = 1,\ n = 2$	1.0000	0.9718	0.0627	−3.0	0.0
Levy flight	$\alpha = 0.7,\ n = 3$	0.7000	0.6817	0.0323	−4.0	−2.0
fBm trajectory	$H = 0.75,\ n = 3$	1.3333	1.3334	0.0302	1.5	2.0
fBm trajectory	$H = 0.5, n = 4$	2.0000	1.9958	0.0203	1.3	1.8
fBm graph	$H = 0.3, n = 1$	1.7000	1.7003	0.0136	0.7	1.5
fBm graph	$H = 0.8, n = 1$	1.2000	1.1677	0.0512	0.8	2.0
Takagi function	$a = 0.75, n = 1$	1.5850	1.5889	0.0169	1.0	1.9
Takagi function	$a = 0.90, n = 1$	1.8480	1.8475	0.0149	1.1	1.8
Logistic map	[25]	0.5000	0.4948	0.0360	0.8	1.4
Rossler oscillator	[26]	2.0100	1.9845	0.0788	0.2	0.9
Lorenz system	[27]	1.2409	1.2388	0.0342	1.2	1.9

lation dimension of the trajectory of an n-dimensional Levy flight with the parameter $\alpha \in (0; 1)$. The lower and the upper boundary for the linear segment were shifted to the left when the theoretical dimension was lower. The graph of the fBm graph was also investigated to determine the efficiency of the D_2 estimator and had a theoretical dimension of $D_2 = 2 - H$. As a representative of the deterministic fractal functions, points from the Takagi function graph were generated. The Takagi function was dependent on the parameter $a \in (1/2; 1)$, and the theoretical correlation dimension was equal to $D_2 = 2 + \log_2 a$. The results from the estimation are shown in Table 5. The representatives of classical dynamic systems were also examined, namely, a logistic map [25] for $r = 3.56995$ with an estimated value of $D_2 = 0.500 \pm 0.005$; a Rossler oscillator [26] for $a = 0.1$, $b = 0.1$ and $c = 14$, with an estimated value of $D_2 = 2.01 \pm 0.01$; and a Lorenz-like system attractor [27] for $\alpha = 51/64$, $\beta = 396/256$ and $\theta = 109/64$, with $D_2 \in [1.2406, 1.2412]$.

8. Conclusion

The asymptotic behaviour of a rotational spectrum was investigated under the assumption of D_2 existence. Rotation in an infinite-dimensional space is recommended for correlation dimension estimation that is based on Monte Carlo simulation. As stated previously, there is a significant difference between traditional correlation integral behaviour and rotational spectrum, which can be seen on the basis of the log-log plot. The effect of spectrum stabilisation for $n \to \infty$ is also useful for D_2 estimation from relatively small uniform samples. However, the proposed method has a disadvantage in the experimental choice of the frequency range for regression, as in the case of the traditional approach.

Acknowledgement

The paper was written with the support of the Czech Technical University in Prague (grant no. SGS14/208/OHK4/3T/14).

References

[1] Edgar G. Measure, topology, and fractal geometry (undergraduate texts in mathematics). Springer; 2013. ISBN 03-877-4748-6.
[2] Falconer KJ. Fractal geometry : mathematical foundations and applications. Chichester: Wiley; 2003. ISBN 04-708-4862-6.
[3] Addison P. Fractals and chaos : an illustrated course. Bristol, UK Philadelphia, Pa: Institute of Physics Pub; 1997. ISBN 9780750304009.
[4] Grassberger P, Procaccia I. Measuring the strangeness of strange attractors. Physica D 1983;9(1–2):189–208. doi:10.1016/0167-2789(83)90298-1.
[5] Grassberger P, Procaccia I. Characterization of strange attractors. Phys Rev Lett 1983;50(5):346–9. doi:10.1103/physrevlett.50.346.
[6] Shayegh F, Sadri S, Amirfattahi R, Ansari-Asl K. A model-based method for computation of correlation dimension, lyapunov exponents and synchronization from depth-EEG signals. Comput Methods Programs Biomed 2014;113(1):323–37. doi:10.1016/j.cmpb.2013.08.014.
[7] Rawal K, Saini BS, Saini I. Adaptive correlation dimension method for analysing heart rate variability during the menstrual cycle. Australas Phys Eng Sci Med 2015;38(3):509–23. doi:10.1007/s13246-015-0369-y.
[8] Kalauzi A, Vuckovic A, Bojić T. Topographic distribution of EEG alpha attractor correlation dimension values in wake and drowsy states in humans. Int J Psychophysiol 2015;95(3):278–91. doi:10.1016/j.ijpsycho.2014.11.008.
[9] Liu Y, Yu Z, Zeng M, Wang S. Dimension estimation using weighted correlation dimension method. Discrete Dyn Nat Soc 2015;2015:1–10. doi:10.1155/2015/837185.
[10] Michalak KP. How to estimate the correlation dimension of high-dimensional signals? Chaos 2014;24(3):033118. doi:10.1063/1.4891185.
[11] Hongying Y, Duanfeng J. Mathematical modelling: v. 2: proceedings of first international conference on modelling and simulation. World Academic Union Ltd; 2008. ISBN 1846260426.
[12] Grafakos L. Classical fourier analysis: graduate texts in mathematics. Springer; 2014. ISBN 1493911937.
[13] Talebinejad M, Chan AD, Miri A, Dansereau RM. Fractal analysis of surface electromyography signals: a novel power spectrum-based method. J Electromyography Kinesiol 2009;19(5):840–50. doi:10.1016/j.jelekin.2008.05.004.
[14] Wen H, Liu Z. Separating fractal and oscillatory components in the power spectrum of neurophysiological signal. Brain Topogr 2015;29(1):13–26. doi:10.1007/s10548-015-0448-0.
[15] Churnside JH, Wilson JJ. Power spectrum and fractal dimension of laser backscattering from the ocean. J Opt Soc Am A 2006;23(11):2829. doi:10.1364/josaa.23.002829.
[16] Debye P. Zerstreuung von röntgenstrahlen. Ann Phys 1915;351(6):809–23. doi:10.1002/andp.19153510606.
[17] Krantz SG. Handbook of complex variables. Birkhäuser; 1999. ISBN 0817640118.
[18] Parzen E. On estimation of a probability density function and mode. Ann Mat Stat 1962;33(3):1065–76. doi:10.1214/aoms/1177704472.
[19] Fischer R. The adaptive resolution concept in form-free distribution estimation. In: Kluge W, editor. Proceedings of the Workshop on Physics and Computer Science. Heidelberg; 1999.
[20] von der Linden VDW, Fischer R. Adaptive kernels and Occam's razor in inversion problems. In: Sears M, Nedeljkovic V, Pendock N, Sibisi S, editors. Proceedings of the Maximum Entropy Conference. NBM printers, Port Elizabeth, South Africa; 1997.
[21] Olson EJ, Robinson JC, Sharples N. Generalised cantor sets and the dimension of products. Math Proc Cambridge Philos Soc 2015;160(01):51–75. doi:10.1017/s0305004115000584.
[22] Hughes BD. Random walks and random environments: volume 1: random walks. Clarendon Press; 1995. ISBN 0198537883.
[23] Wu DS, Xiao YM. Dimensional properties of fractional brownian motion. Acta Math Sin Engl Ser 2007;23(4):613–22. doi:10.1007/s10114-005-0928-3.
[24] Takeo F. Box-counting dimension of graphs of generalized takagi series. Jpn J Ind Appl Math 1996;13(2):187–94. doi:10.1007/bf03167241.
[25] Grassberger P, Procaccia I. Measuring the strangeness of strange attractors. Physica D 1983;9(1–2):189–208.
[26] Peitgen H-O, Jürgens H, Saupe D. Chaos and fractals: new frontiers of science. Springer; 1993. ISBN 0387979034.
[27] Galatolo S, Nisoli I. Rigorous computation of invariant measures and fractal dimension for maps with contracting fibers: 2d lorenz-like maps. Ergodic Theor Dynam Syst 2015;36(06):1865–91. doi:10.1017/etds.2014.145.